ADVANCED FUNCTIONAL MATERIALS

FULL PAPER

DOI: 10.1002/adfm.200800135

Directed Self-Assembly of Gradient Concentric Carbon Nanotube Rings**

By *Suck Won Hong, Wonje Jeong, Hyunhyub Ko, Michael R. Kessler, Vladimir V. Tsukruk,* and *Zhiqun Lin**

Hundreds of gradient concentric rings of linear conjugated polymer, (poly[2-methoxy-5-(2-ethylhexyloxy)-1,4- phenylenevinylene], i.e., MEH-PPV) with remarkable regularity over large areas were produced by controlled "stick-slip" motions of the contact line in a confined geometry consisting of a sphere on a flat substrate (i.e., sphere-on-flat geometry). Subsequently, MEH-PPV rings were exploited as a template to direct the formation of gradient concentric rings of multiwalled carbon nanotubes (MWNTs) with controlled density. This method is simple, cost effective, and robust, combining two consecutive self-assembly processes, namely, evaporation-induced self-assembly of polymers in a sphere-on-flat geometry, followed by subsequent directed self-assembly of MWNTs on the polymer-templated surfaces.

1. Introduction

Spontaneous self-assembly of nanoscale materials to form well ordered, often intriguing complex structures via irreversible solvent evaporation from a solution containing nonvolatile solutes (e.g., nanoparticles, colloids, and DNA) provides a simple route to functional materials.[1–11] When compared with other conventional techniques (e.g., photolithography, e-beam lithography, soft-lithography, and nanoimprint lithography), the surface patterning by controlled solvent evaporation is simple and cost-effective. It offers a means of organizing materials on the nanoscale into ordered microscopic structures without the need for lithography or an external field over large surface areas using a facile routine.

Carbon nanotubes (CNTs) have been widely recognized as a potential material for use as semiconducting or conducting elements in nanoelectronics, sensors, and nanoscale transistors due to their outstanding electrical, optical, mechanical, and structural properties.[12–23] The physicochemical properties of CNT-based materials strongly depend on the order and orientation of CNTs.[14,15,24–28] To this end, impressive recent studies have centered on developing techniques for patterning and depositing CNTs on the surface by arranging them into well-ordered arrays with controlled coverage, including electric-field-assisted growth,[29,30] the use of controlled flocculation in laminar microfluidic networks,[14] selective laser ablation,[24] guided chemical vapor deposition growth on single-crystal quartz substrates using patterned stripes of iron catalyst,[31] and blown bubble film process[32] to fabricate nanotube-based devices, e.g., high density sensor arrays and thin film transistors.[31–34] Successful implementation of CNTs also requires strategies to deposit and pattern CNTs over large areas, which still remains challenging especially if gradient variation of patterning (e.g., spacing) is desirable.

Recently, self-organized gradient concentric ring patterns have been produced by confining a drop of polymer solution in a restricted geometry composed of a sphere on a flat surface.[35–43] Rather than allowing the solvent to evaporate over the entire droplet area as in copious past work, in which droplets evaporated from a single surface,[44–46] the evaporation was restricted at the droplet edges.[35,36] Concentric rings were formed by controlled, repetitive pinning and depinning of the contact line (i.e., "stick-slip" motion).[35,36] However, to the best of our knowledge, gradient concentric rings composed of CNTs with unprecedented regularity have not been reported to date. CNTs organized in a gradient concentric ring mode may offer possibilities for mass production of CNT-based electronic devices to explore the channel length effect on the mobility of CNTs in one step.

Herein, we present a simple and straightforward method to create gradient concentric rings of CNTs over very large surface areas by combining two consecutive self-assembly processes. Hundreds of gradient concentric polymer rings with remarkable regularity were spontaneously formed on Si substrate via evaporation-induced self-assembly of polymer in a confined geometry consisting of a sphere on a flat Si substrate (Fig. 1). The concentric polymer rings on the Si were then exploited as a chemically patterned surface to guide the formation of multiwalled carbon nanotube (MWNT) rings

[*] Prof. Z. Q. Lin, S. W. Hong, W. Jeong, Prof. M. R. Kessler
Department of Materials Science and Engineering
Iowa State University
Ames, IA 50011 (USA)
E-mail: zqlin@iastate.edu
H. Ko, Prof. V. V. Tsukruk
School of Materials Science and Engineering, Georgia Institute of Technology
Atlanta GA 30332 (USA)

[**] We gratefully acknowledge support from the National Science Foundation (CBET-0730611) and the 3M non-tenured faculty award. We also thank Qingze Zou for AFM usage. Supporting Information is available online from Wiley InterScience or from the authors.

WILEY InterScience DISCOVER SOMETHING GREAT

© 2008 WILEY-VCH Verlag GmbH & Co. KGaA, Weinheim

ADVANCED FUNCTIONAL MATERIALS

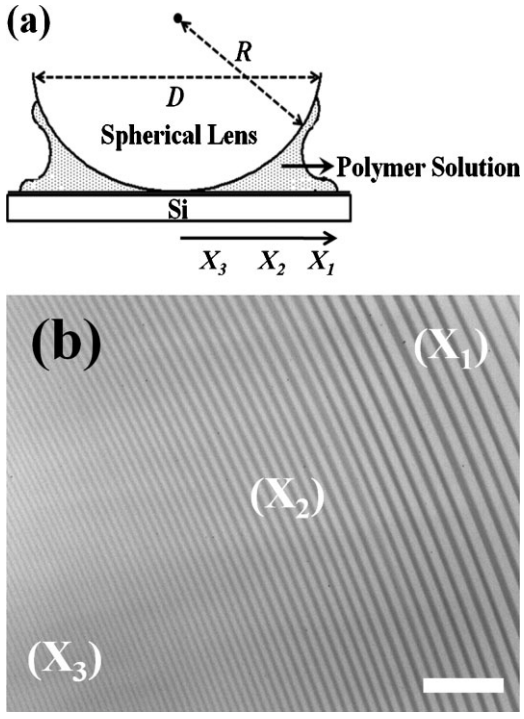

Figure 1. a) Schematic illustration of a drop of polymer solution trapped between a sphere and a Si substrate (i.e., a sphere-on-flat geometry), forming a capillary-held polymer solution. During the course of solvent evaporation, concentric rings composed of polymer were formed by controlled, repetitive ''stick-slip'' motion of the contact line. X_1, X_2, and X_3 are the distances of ring away from the sphere/Si contact center at outermost region (X_1), intermediate region (X_2), and innermost region (X_3), respectively. b) Optical micrograph of gradient concentric MEH-PPV rings formed in the sphere-on-flat geometry (Fig. 1a). A decrease in center-to-center distance between the rings, λ_{C-C} with increasing proximity to the center of sphere/Si contact (i.e., from location X_1 to X_2 to X_3 (Fig. 1a)) is clearly evident. Scale bar = 200 μm.

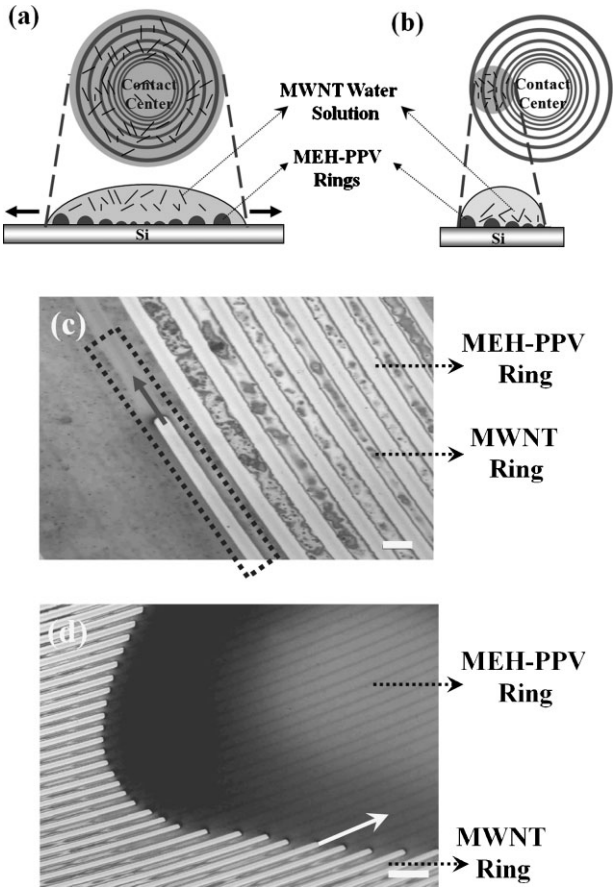

Figure 2. a) and b) Methods used to cast the MWNT/PDDA water solution ($c = 0.05$ mg ml^{-1}). (a) Solution overspread the entire surface of ring patterns (*Method a*). b) Solution covered only a small part of ring pattern (*Method b*).(c) Optical micrograph during the formation of MWNT rings by *Method a*. The water meniscus retreated along the MEH-PPV ring surface (i.e., dewetting on hydrophobic MEH-PPV ring), as indicated by an arrow in a dashed box, thereby forming two MWNT rings adjacent to each other. Scale bar = 30 μm. d) Optical micrograph during the formation of MWNT rings by *Method b*. The solution was confined within the MEH-PPV rings. As water evaporated (direction indicated by an arrow), a periodic family of MWNT rings were left behind on the Si substrate. Scale bar = 70 μm.

(i.e., directed self-assembly). Specifically, a drop of water-dispersed MWNTs mixed with poly (diallyl dimethylammonium) chloride (PDDA) was cast on the surface of the template polymer rings. The periodically alternating hydrophobic polymer rings and hydrophilic Si substrate (i.e., Si rings) provided different wettabilities for the MWNT/PDDA solution. As water evaporated, the MWNT solution dewetted the polymer rings while forming MWNT rings on the Si rings. The combination of spontaneous *evaporation-induced self-assembly* and subsequent *directed self-assembly* offers a new means of patterning microscopic CNT rings *over large areas*. This method is fast and cost-effective, eliminating the need for multistage lithography and externally applied forces.

2. Results and Discussion

In the evaporation-induced self assembly (where MEH-PPV toluene solution was loaded between a spherical lens and a Si substrate (Fig. 1a)), evaporative loss of toluene at the capillary edge triggered the pinning of the contact line (i.e., ''stick''). The outermost MEH-PPV ring was thus formed. During the deposition of MEH-PPV, the initial contact angle of the capillary edge decreased gradually due to evaporation of toluene to a critical angle, at which the capillary force (depinning force) becomes larger than the pinning force.[36] This caused the contact line to jump to a new position (i.e., ''slip''), and a new ring was developed.[35,36,44] Repeated pinning and depinning cycles of the contact line led to the formation of gradient concentric rings of MEH-PPV (Fig. 1b). Notably, the center to center distance between adjacent rings, λ_{C-C} decreased with increased proximity to the sphere/Si contact center (i.e., from X_1 to X_3), which can be attributed to the competition between linear pinning force and nonlinear capillary force.[36] At the outermost region, X_1, both λ_{C-C} and MEH-PPV ring height, $h_{MEH-PPV}$ decreased progressively

 © 2008 WILEY-VCH Verlag GmbH & Co. KGaA, Weinheim

from $\lambda_{C-C} = (20.4 \pm 0.3)$ μm, $h_{MEH\text{-}PPV} = (14.8 \pm 0.4)$ nm ($X_1 \cong$ 4100 μm in Fig. 1b) to (11.2 ± 0.3) μm and (7.6 ± 0.4) nm at the intermediate region ($X_2 \cong 3500$ μm in Fig. 1b) to (4.3 ± 0.3) μm and (1.6 ± 0.3) nm at the innermost region ($X_3 \cong 2700$ μm in Fig. 1b), as measured by atomic force microscope (AFM). Only a small zone of the entire gradient concentric ring pattern is shown in Figure 1b. The entire ring pattern was formed over $\pi\left(\frac{D'}{2}\right)^2 = \pi(8/2)^2 = 50.24\,\text{mm}^2$ surface areas, where D' is the diameter of the outermost ring in the present study ($D' = 8$ mm), dictated by the volume of the MEH-PPV solution and the diameter of the spherical lens used, D ($D = 1$ cm in Fig. 1a). The axially symmetric sphere-on-flat geometry provides a unique environment (i.e., a bound solution) for controlling the flow within an evaporating droplet, which in turn regulates the structure formation.[35–41] Thus, in sharp contrast to the irregular concentric rings formed due to stochastic ''stick-slip'' cycles of the contact line when a droplet evaporates from a single surface (i.e., an unbound solution),[44,45,47,48] highly ordered, gradient concentric rings of MEH-PPV are produced using the sphere-on-flat geometry.

Gradient concentric MEH-PPV rings are intriguing templates to guide self-assembly of nanoscale materials, i.e., MWNTs, as schematically illustrated in Figure 2. The pristine MWNTs showed poor dispersibility in water. To improve the water solubility, the MWNT surface was functionalized with carboxylic acid groups (–COOH) via repeated oxidation and ultrasonication treatment (see Experimental). The 0.5 wt % positively charged poly (diallyl dimethylammonium) chloride (PDDA) was added to the MWNT solution to further improve the water dispersibility and enhance the adhesion of MWNTs to the Si substrate[49] before drop-casting the solution onto the MEH-PPV ring-patterned Si substrate using *Method a* and *Method b*. In *Method a*, the droplet was free to spread on Si outside the MEH-PPV rings, during which the contact angle decreased without the pinning of the contact line while the droplet maintained the circular shape. As a result, the solution film thickness reduced to a thickness comparable to the height of MEH-PPV rings during water spreading and evaporation. The periodically alternating hydrophobic MEH-PPV ring and hydrophilic Si substrate between the MEH-PPV rings (i.e., Si

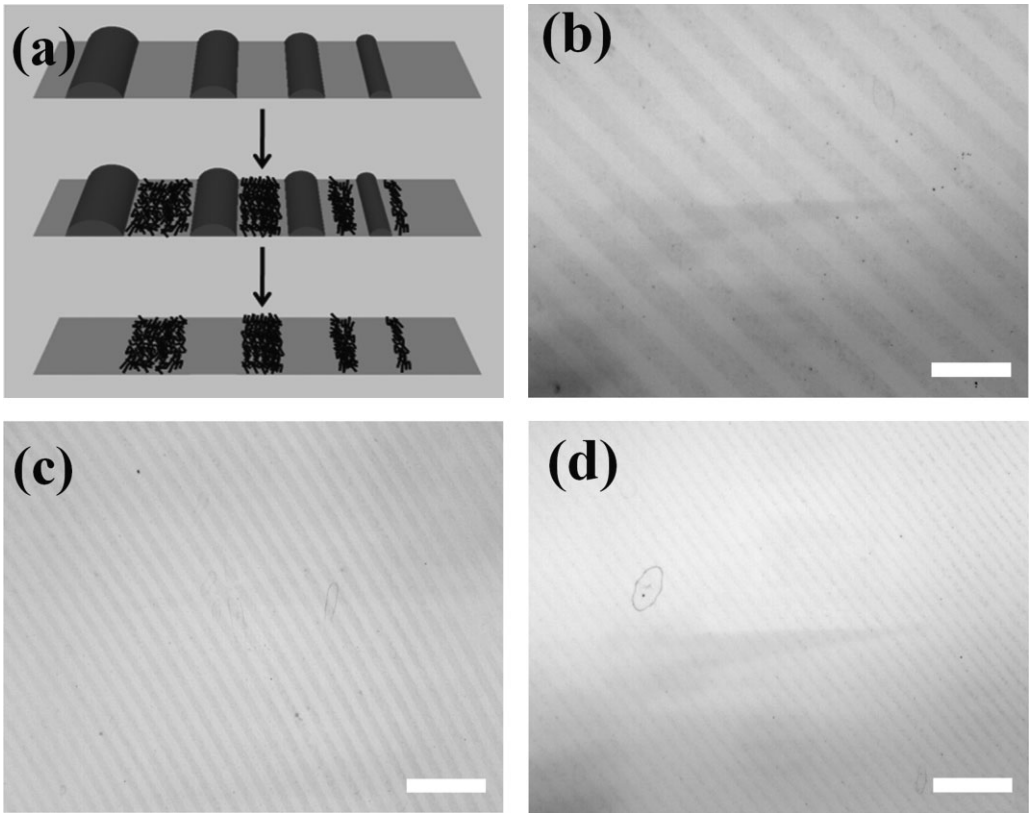

Figure 3. a) Schematic stepwise representation of formation of gradient concentric MWNT rings. Evaporation-induced self-assembly of MEH-PPV rings on Si substrate from MEH-PPV toluene solution in sphere-on-flat geometry, showing a decrease in λ_{C-C} and height of the rings, h, from outermost ring (left) toward the original sphere/Si contact center (right) (first panel). Then a drop of MWNT/PDDA water solution was drop-cast onto the MEH-PPV ring-patterned Si substrate. Upon completion of water evaporation, MWNT rings were formed in between MEH-PPV rings (second panel). After selective removal of MEH-PPV with toluene, gradient concentric MWNT rings can be revealed (last panel). b)–d) Optical micrographs of highly ordered, gradient MWNT rings on Si substrate over large areas produced by template-assisted self-assembly as described in (a) (*Method a*). The locations of MWNT rings corresponding to original MEH-PPV templates are (a) at X_1, (b) at X_2, and (c) at X_3 (Fig. 1b), respectively. Scale bars = 45 μm.

© 2008 WILEY-VCH Verlag GmbH & Co. KGaA, Weinheim

ADVANCED FUNCTIONAL MATERIALS

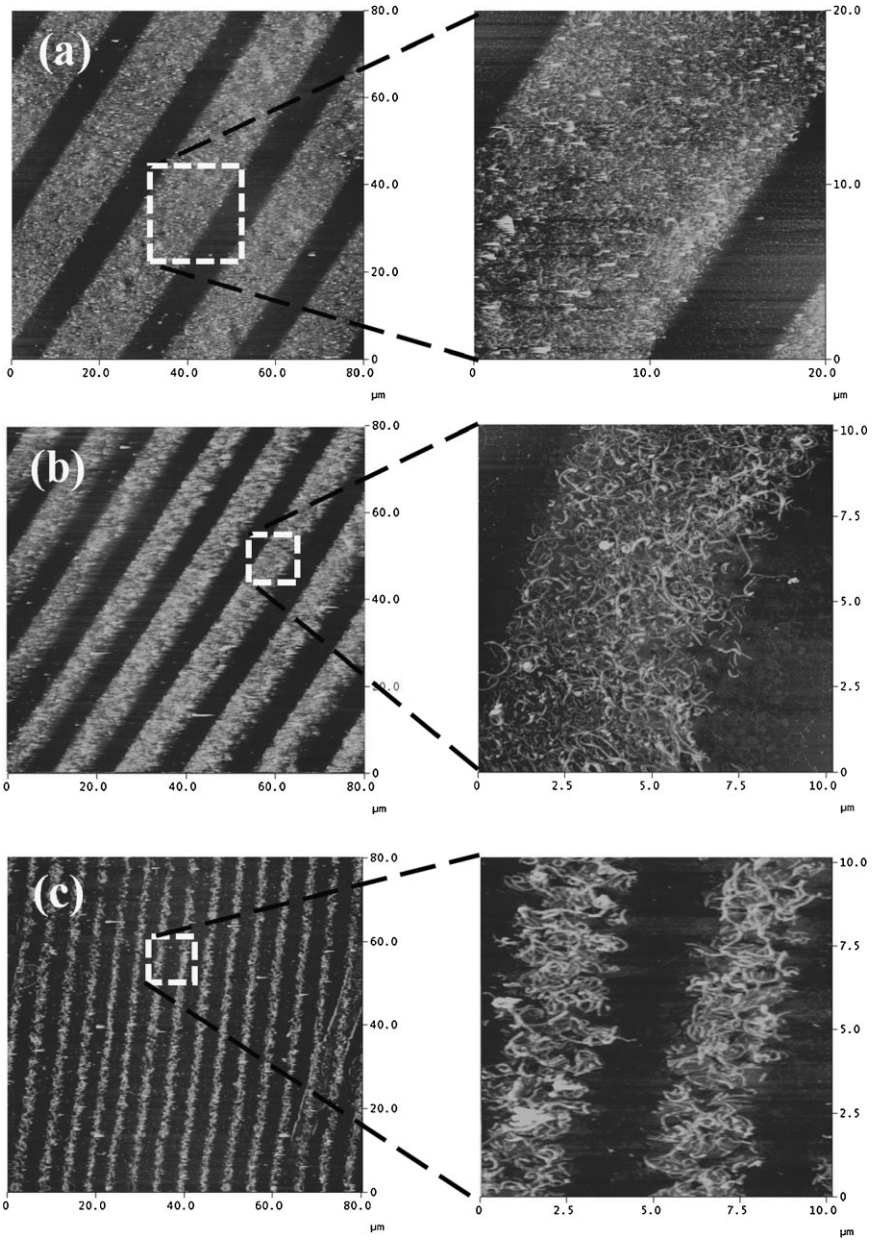

Figure 4. AFM height images corresponding to optical micrographs shown in Figure 3b–d. a) at outermost region, X_1, b) at intermediate region, X_2, and c) at innermost region X_3. Close-ups of individual ring are shown in the right panel, in which MWNTs formed random network and were densely packed. The image size is $80 \times 80\ \mu m^2$ for the left panels, $20 \times 20\ \mu m^2$ for the right panel of (a), $10 \times 10\ \mu m^2$ for the right panel of (b) and (c). The z scale is 50 nm for all images.

rings) provided different wettabilities for the MWNT/PDDA solution. The interaction between hydrophilic MWNT/PDDA and hydrophilic Si facilitated the deposition of MWNTs onto Si rings, while MWNT/PDDA dewetted hydrophobic MEH-PPV rings. As water evaporated, the water meniscus receded from the MEH-PPV rings (the arrow in Fig. 2c), driven by the capillary force. The MWNTs were pushed to Si rings in a direction perpendicular to the receding water front as a result of evaporation-induced capillary flow. Furthermore, the electrostatic interaction between positively charged PDDA and negatively charged MWNT promoted both CNT-CNT electrostatic repulsion and CNT hydrophilicity.[49] The electrostatic interaction between SiO^- groups and the positively charged PDDA enhanced MWNT adhesion to the Si substrate to form a uniform ring.[49–51] The synergy of capillary force and electrostatic interaction effectively directed the self-assembly of the MWNTs onto the Si rings over the entire MEH-PPV template.

In *Method b*, where a drop of MWNT/PDDA solution covered only a small part of MEH-PPV ring pattern, the

 © 2008 WILEY-VCH Verlag GmbH & Co. KGaA, Weinheim

droplet maintained its circular shape and was confined within hydrophobic concentric rings, resulting in a larger, fixed contact angle than in *Method a* (Fig. 2b). During water evaporation the water meniscus retreated along concentric MEH-PPV rings driven by the capillary force, leaving behind rake-like MWNTs deposited on the Si rings as shown in the left portion of Figure 2d. The MWNTs were tethered to Si rings through the electrostatic interaction facilitated by positively charged PDDA (i.e., forming a MWNTs/PDDA/Si layer).[49–51]

The dimension of the microscopic concentric MWNT rings was significantly affected by the geometric constraints imposed by the MEH-PPV rings. Due to the gradient nature of the template of MEH-PPV rings, gradient concentric MWNT rings were achieved after selective removal of MEH-PPV with toluene, as schematically illustrated in Figure 3a. Figure 3b–d shows optical micrographs of gradient concentric MWNT rings obtained (via *Method a*), corresponding to the location of original MEH-PPV rings at the outermost (X_1), intermediate (X_2), and innermost (X_3) regions, respectively, from Figure 1b. The size and shape of the MWNT rings was highly complementary to those of original MEH-PPV rings and were not disrupted during the successive dissolving of MEH-PPV with toluene.

To quantify the dimension of adsorbed MWNT rings in Figure 3b–d, AFM measurements were performed. Figure 4 shows AFM height images corresponding to optical micrographs in Figure 3b–d. Locally, the rings appear as parallel stripes. The number of stripes in the $80 \times 80\ \mu m^2$ scanning area increases from 5 (left panel in Fig. 4a) to 9 (Fig. 4b) to 16 (Fig. 4c). Section analysis of these AFM images revealed that the width of rings, w decreased from $w = (15.1 \pm 0.3)\ \mu m$ at X_1, to $w = (8.2 \pm 0.3)\ \mu m$ at X_2, to $w = (2.5 \pm 0.2)\ \mu m$ at X_3 (see Supporting Information). This correlated well with the values obtained from the template of MEH-PPV rings. The thickness of MWNTs, h_{MWNT} was rather constant in all locations (i.e., $h_{MWNT} \cong 19$ nm in X_1, X_2, and X_3), suggesting the formation of a monolayer of MWNT on the Si substrate given that the thickness of a MWNT was approximately 20 nm, as determined by TEM (Fig. 5).

Further scrutiny of each individual MWNT ring obtained by *Method a* revealed a random network of densely packed MWNTs (right panels in Fig. 4). The formation of a random network of MWNTs can be rationalized as follows. Complete water evaporation from MEH-PPV ring-patterned Si substrate was over a course of 4 h, rather than 30 min as in the case of MEH-PPV in which toluene was used. Thus, the evaporation-induced capillary flow was slow and could not orient the MWNT along the flow direction during the drying process. Consequently, the MWNTs were randomly dispersed within a ring.

Figure 6 shows the optical micrograph and AFM images of MWNT rings formed at the region in between X_1 and X_2 prepared by *Method b*. In comparison to monolayer of MWNT rings produced by *Method a* (Fig. 4), densely packed MWNT bundles were observed (Fig. 6b–d), manifested in a larger value

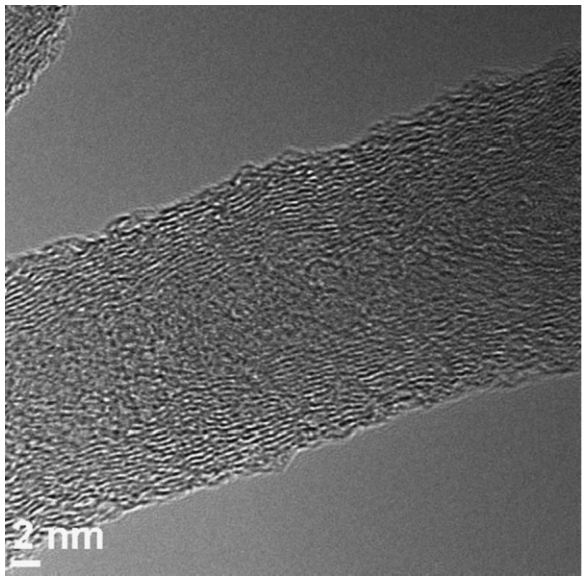

Figure 5. TEM image of a MWNT with a thickness of 20 nm.

of thickness, $h_{MWNT} \cong 42$ nm (see Supporting Information). This is attributed to the larger initial contact angle formed by using *Method b* as depicted in Figure 2b. A larger contact angle due to unfavorable interfacial interaction between hydrophobic MEH-PPV rings and hydrophilic MWNT/PDDA allowed more MWNTs to deposit on Si rings, thereby yielding thicker, densely packed MWNTs. The width of the rings was 4.0 μm, smaller than 8.2–15.1 μm (corresponding to the width in X_1 and X_2 regions) values obtained using *Method a*. This may be explained by the fact that, due to larger initial contact angle, the MWNTs deposited on Si rings right after the solution front receded from the MEH-PPV rings while the deposition was still liquid-like. The residual amount of water in the liquid-like MWNT rings further evaporated and retracted in a direction perpendicular to the ring from both edges, thereby leading to rings with a smaller width. This perpendicular flow may partially contribute to the larger thickness of the MWNTs obtained (Fig. 6c and d and Supporting Information). This process also promoted the ordering of MWNTs inside the microscopic ring. The orientation of MWNTs within the ring was improved (i.e., aligned along the ring in Fig. 6d) as compared with rings obtained by *Method a* in which MWNTs formed a random network (Fig. 4).

To further verify the formation of periodic MWNT rings, Raman mapping was conducted. For the MWNT rings produced by *Method a*, the high-resolution Raman mapping obtained with typical Raman G mode of MWNT ($1586\ cm^{-1}$) at three different locations (i.e., X_1, X_2, and X_3 in Fig. 1a) confirmed the formation of gradient concentric MWNT rings with decreased periodicity as clearly evidenced in Figure 7. The contrast of Raman image reflects the monolayer coverage of MWNTs produced by *Method a*. On the other hand, the densely-packed MWNT rings formed by *Method b* exhibited much higher contrast in optical microscope image (Fig. 8a) and

© 2008 WILEY-VCH Verlag GmbH & Co. KGaA, Weinheim

ADVANCED FUNCTIONAL MATERIALS

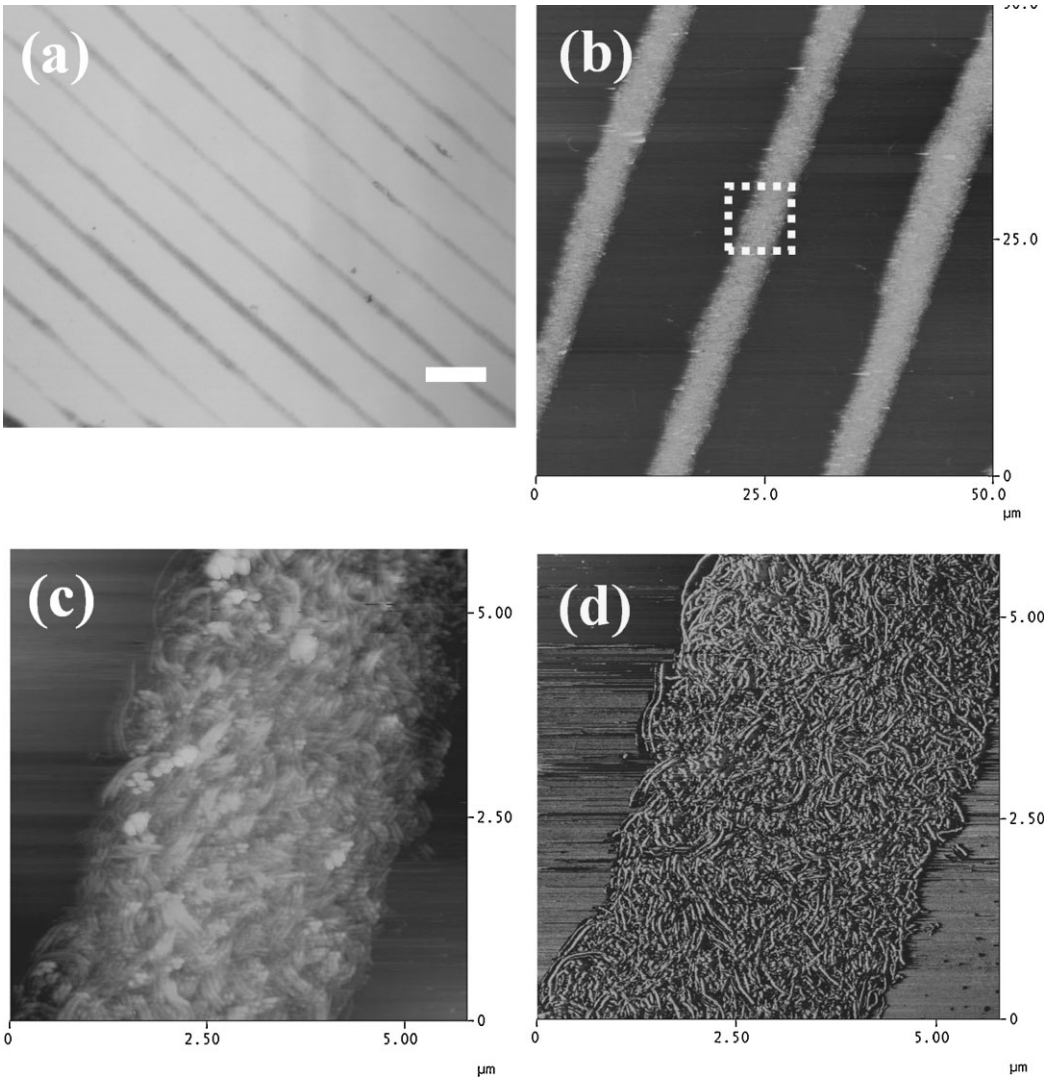

Figure 6. a) Optical micrograph of highly ordered MWNT rings at the region in between X_1 and X_2 produced by *Method b*. Locally, they appeared as parallel stripes. Scale bar = 20 μm. b) Corresponding AFM height image. c) and d) The close-up AFM images marked in (b), where (c) and (d) are phase and height images, respectively. Densely packed MWNTs bundles are clearly evident in (d). The image size is 50 × 50 μm^2 in (b), and 5.8 × 5.8 μm^2 in (c) and (d). The *z* scale is 50 nm for all images.

corresponding Raman mapping (Fig. 8b). The well-defined MWNT rings visible in the Raman G mode provided enhanced contrast in Raman intensity variation across eight MWNT rings (Fig. 8b) as compared to that of monolayer MWNT rings in Figure 7. The presence of intense Raman peaks on the MWNT rings while zero counts in between the MWNT rings (i.e., on the Si rings) validated that there were no MWNTs on the Si rings which were formed after the removal of MEH-PPV rings (Fig. 8c). This was consistent with optical microscopy observation (Fig. 8a).

It is noteworthy that, rather than highly regular concentric MWNT rings, irregular MWNT spokes were formed in a direction parallel to the movement of the solution front when the MWNT/PDDA solution was directly allowed to evaporate from the sphere-on-flat geometry.

3. Conclusions

In summary, we have demonstrated that the use of sphere-on-flat geometry provides remarkable control over the evaporative flux, thereby leading to evaporation-induced self-assembly of gradient concentric rings of polymers with unprecedented regularity by repeated ''stick-slip'' cycles of the contact line. Subsequently, the polymeric rings were exploited as a template to direct self assembly of MWNTs from the water solution (i.e., deposition on hydrophilic Si substrate and dewetting on hydrophobic polymer rings). After water evaporation followed by selective removal of the template of polymer rings, gradient concentric MWNT rings over very large areas were achieved (i.e., 50 mm^2 in the present study, which was dictated by the initial volume of polymer solution

 © 2008 WILEY-VCH Verlag GmbH & Co. KGaA, Weinheim

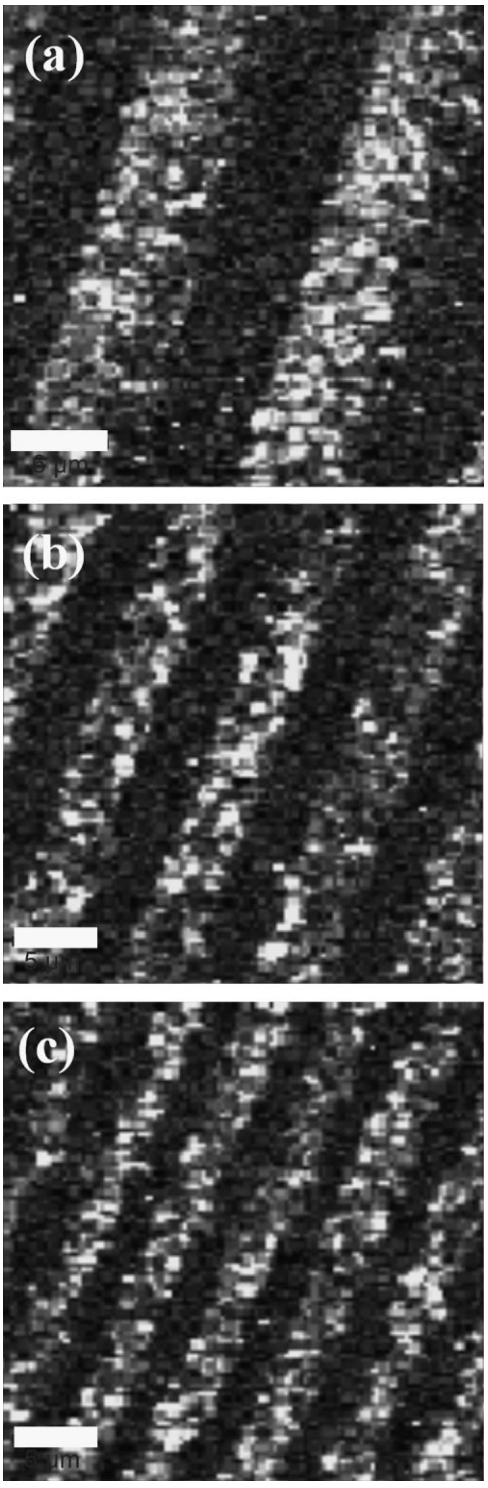

Figure 7. Raman images of MWNT rings on Si substrate produced by *Method a*, acquired by integration of Raman intensity at G mode (1586 cm^{-1}); a) at outermost region, X_1, b) at intermediate region, X_2, and c) at innermost region X_3. The scale bars are 6 μm, 5 μm, and 5 μm in (a), (b), and (c), respectively. The Raman intensity varied from dark (low) to bright (high) color.

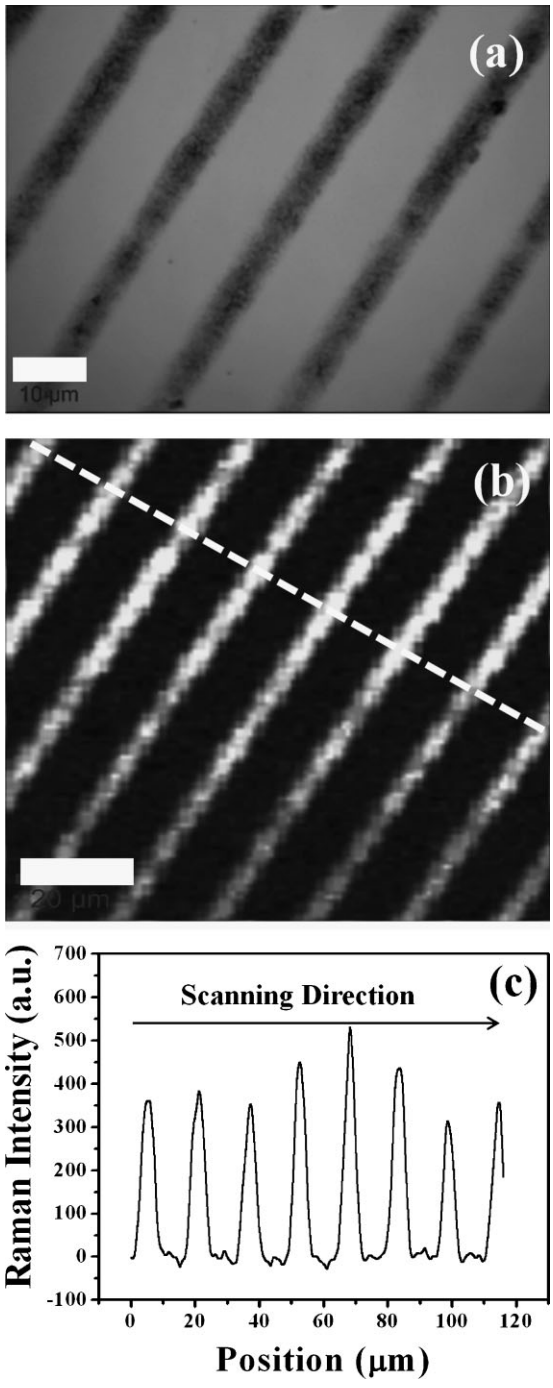

Figure 8. a) Optical micrograph of MWNT rings produced by *Method b*. b) Corresponding Raman image acquired by integration of Raman intensity at G mode (1586 cm^{-1}). The Raman intensity varies from dark (low) to bright (high) color. c) The Raman intensity variation at G mode across the MWNT rings on Si substrate. The measurements were performed in a direction perpendicular to the ring pattern as indicated by a white dotted line in Raman image (b). The scale bars are 10 μm and 20 μm in (a) and (b), respectively.

© 2008 WILEY-VCH Verlag GmbH & Co. KGaA, Weinheim

ADVANCED FUNCTIONAL MATERIALS

loaded and the diameter of spherical lens used, D. By increasing D and placing a larger amount of polymer solution, MWNT rings with even larger areas can ultimately be achieved). The spacing, width, and height of MWNT rings can be finely tailored by using different casting methods. This facile technique opens up a new avenue for high throughput, lithography- and external field-free patterning of microscopic CNT rings over large areas. We envisage that, by replacing MWNTs with single-walled carbon nanotubes (SWNTs), the formation of gradient concentric SWNT rings from solution-based SWNTs may be suitable for applications in electrics, optics, and sensors, for example, mass production of SWNT-based electronic devices to explore the channel length effect on the mobility of SWNTs in one step.

4. Experimental

Evaporation-Induced Self-Assembly of MEH-PPV Rings in a Sphere-on-Flat Geometry: Linear conjugated polymer, poly[2-methoxy-5-(2-ethylhexyloxy)-1,4-phenylenevinylene] (MEH-PPV; molecular weight = 50–300 kg mol^{-1}; American Dye Sources) was selected as the nonvolatile solute to prepare a 0.075 mg ml^{-1} MEH-PPV toluene solution. Si wafers and spherical lenses made from fused silica (the radius of curvature, $R = 1.65$ cm, and the diameter, $D = 1$ cm (Fig. 1a)) were cleaned with a mixture of sulfuric acid and Nochromix. They were rinsed extensively with DI water and then blown dry with N_2. A sphere-on-flat geometry was constructed and implemented as follows. Both the spherical lens and Si substrate were firmly fixed at the top and bottom of sample holders, respectively. An inchworm motor was used to bring the upper sphere into near contact with lower stationary Si substrate. Before contact, with just a few hundred micrometers between the surfaces, 20 μL of MEH-PPV toluene solution was loaded and trapped between the sphere and Si due to capillary forces. The sphere was finally moved into contact with the Si substrate. Thus, a capillary-held MEH-PPV toluene solution was formed with evaporation rate highest at the extremity, as schematically illustrated in Figure 1a. This geometry led to a controlled, repetitive "stick-slip" motion of the three phase contact line, which moved toward the sphere/Si contact center (Fig. 1a) during the course of toluene evaporation. As a result, gradient concentric MEH-PPV rings were formed on both the spherical lens and the Si substrate. Only the ring patterns formed on the Si substrate were utilized as templates in this study (Fig. 1b).

Directed Self-Assembly of Gradient Concentric MWNT Rings: To prepare oxidized MWNTs (i.e., MWNTs with surface and end carboxyl groups), as-supplied MWNTs (20 mg, O.D. × I.D., 15–20 nm × 5–10 nm; Sigma–Aldrich) were added to nitric acid (60%, 30 ml), and sonicated for 10 min for initial dispersion, followed by a 12 h reflux at 130 °C. The dispersion was cooled to room temperature and filtered using a 1-μm-pore PTFE membrane filter. The purified MWNTs were rinsed extensively with DI water. The reflux with nitric acid produced carboxyl, hydroxyl, and carbonyl groups at the defect sites of the MWNTs. Subsequently, purified MWNTs were dispersed in DI water again and further oxidized with potassium permanganate perchloric acid solution [52–54]. Finally, the dispersion was filtered and rinsed with HCl solution. As a result, carboxylic acid functionalized MWNTs were obtained (i.e., MWNT-COOH; 14 mg) [55] and dried at 70 °C under vacuum for 24 h. A 0.05 mg ml^{-1} MWNT-COOH DI water solution was prepared after ultrasonication for 1 h. To improve the processibility and facilitate electrostatic compatibility, 25 μL of 20% aqueous positively charged polyelectrolyte, poly(diallyl dimethylammonium) chloride (PDDA, molecular weight = 200–350 kg mol^{-1}; Aldrich) was added into the above mentioned 0.25 mg MWNT in 5 ml DI water. The MWNT/PDDA water solution was cast on the MEH-PPV ring-patterned Si substrate by two different methods: overspreading the entire MEH-PPV ring patterned surface (*Method a*) and partially covering the MEH-PPV rings (*Method b*) as depicted in Figure 2a and b, respectively. In *Method a*, a 50 μl drop of the MWNT/PDDA water solution was cast at the center of the MEH-PPV rings. The solution spread freely and exceeded the outermost MEH-PPV ring (Fig. 2a). In *Method b*, only a 10 μl drop of solution was applied on the top of MEH-PPV rings locally and was trapped between the inner- and outer-most rings (Fig. 2b). The experiments were performed inside a sealed chamber. It took about 4 h and 8 h to allow the water to completely evaporate in *Method a* and *Method b*, respectively. After drying, the samples were immersed in toluene for 40 min to selectively dissolve the MEH-PPV rings. Finally, the samples were rinsed extensively with ethanol, sonicated for 1 min, and blow-dried with N_2.

Characterizations: An Olympus BX51 optical microscope (OM) in the reflection mode was used to investigate the ring patterns deposited on the Si substrate. Atomic force microscopy (AFM) images of the rings were obtained using a Digital instruments Dimension 3100 scanning force microscope in the tapping mode. BS-tap300 tips from Budget Sensors with spring constants ranging from 20 to 75 N m^{-1} were used as scanning probes. Raman measurements were performed (confocal Raman microscope alpha300R (WiTec); excited with a 514 nm Ar^+ laser at 4 mW) to confirm the formation of periodic MWNT rings. A Raman mapping of MWNT rings was acquired by using 100 × objective and integration time of 0.2–1 s for each 360 × 360 nm pixel in Raman image.

Received: January 26, 2008
Revised: March 7, 2008

[1] J. Huang, F. Kim, A. R. Tao, S. Connor, P. D. Yang, *Nat. Mater.* **2005**, *4*, 896.
[2] J. Huang, R. Fan, S. Connor, P. D. Yang, *Angew. Chem. Int. Ed.* **2007**, *46*, 2414.
[3] J. Huang, A. R. Tao, S. Connor, R. He, P. D. Yang, *Nano Lett.* **2006**, *6*, 524.
[4] M. Gleiche, L. F. Chi, H. Fuchs, *Nature* **2000**, *403*, 173.
[5] T. P. Bigioni, X. M. Lin, T. T. Nguyen, E. I. Corwin, T. A. Witten, H. M. Jaeger, *Nat. Mater.* **2006**, *5*, 265.
[6] E. Rabani, D. R. Reichman, P. L. Geissler, L. E. Brus, *Nature* **2003**, *426*, 271.
[7] B. P. Khanal, E. R. Zubarev, *Angew. Chem. Int. Ed.* **2007**, *46*, 2195.
[8] J. Guan, L. J. Lee, *Proc. Natl. Acad. Sci. USA* **2005**, *102*, 18321.
[9] V. V. Tsukruk, H. Ko, S. Peleshanko, *Phys. Rev. Lett.* **2004**, *92*, 065502.
[10] C. P. Martin, M. O. Blunt, E. Pauliac-Vaujour, A. Stannard, P. Moriarty, *Phys. Rev. Lett.* **2007**, *99*, 116103.
[11] H. Ko, S. Peleshanko, V. V. Tsukruk, I. Vancea, U. Thiele, *J. Phys. Chem. B* **2004**, *108*, 4385.
[12] S. Iijima, *Nature* **1991**, *354*, 56.
[13] P. M. Ajiyan, *Chem. Rev.* **1999**, *99*, 1787.
[14] J.-U. Park, M. A. Meitl, S.-H. Hur, M. L. Usrey, M. S. Strano, P. J. A. Keins, J. A. Rogers, *Angew. Chem. Int. Ed.* **2006**, *45*, 581.
[15] S. G. Rao, L. Huang, W. Setyawan, S. Hong, *Nature* **2003**, *425*, 36.
[16] R. H. Baughman, A. A. Zakhidov, W. A. de Heer, *Science* **2002**, *297*, 787.
[17] A. A. Mamedov, N. A. Kotov, M. Prato, D. M. Guldi, J. P. Wicksted, A. Hirsch, *Nat. Mater.* **2002**, *1*, 190.
[18] P. M. Ajayan, *Chem. Rev.* **1999**, *99*, 1787.
[19] D. Mann, Y. K. Kato, A. Kinkhabwala, E. Pop, J. Cao, X. Wang, L. Zhang, Q. Wang, J. Guo, H. Dai, *Nat. Nanotechnol.* **2007**, *2*, 33.

 © 2008 WILEY-VCH Verlag GmbH & Co. KGaA, Weinheim

[20] C. Y. Li, L. Y. Li, W. W. Cai, S. L. Kodjie, K. K. Tenneti, *Adv. Mater.* **2005**, *17*, 1198.
[21] W. Song, I. A. Kinloch, A. H. Windle, *Science* **2003**, *302*, 1363.
[22] S. J. Oh, Y. Cheng, J. Zhang, H. Shimoda, O. Zhou, *Appl. Phys. Lett.* **2003**, *82*, 2521.
[23] H. Shimoda, S. J. Oh, H. Z. Geng, R. J. Walker, X. B. Zhang, L. E. McNeil, O. Zhou, *Adv. Mater.* **2002**, *14*, 899.
[24] C. Kocabas, M. A. Meitl, A. Gaur, M. Shim, J. A. Rogers, *Nano Lett.* **2004**, *4*, 2421.
[25] R. Sharma, C. Y. Lee, J. H. Choi, K. Chen, M. S. Strano, *Nano Lett.* **2007**, *7*, 2693.
[26] C. Kocabas, N. Pimparkar, O. Yesilyurt, S. J. Kang, M. A. Alam, J. A. Rogers, *Nano Lett.* **2007**, *7*, 1195.
[27] H. Ko, V. V. Tsukruk, *Nano Lett.* **2006**, *6*, 1443.
[28] Y. Wang, D. Maspoch, S. Zou, G. C. Schatz, R. E. Smalley, C. A. Mirkin, *Proc. Natl. Acad. Sci. USA* **2006**, *103*, 2026.
[29] Y. Zhang, A. Chang, J. Cao, Q. Wang, W. Kim, Y. Li, N. Morris, E. Yenilmez, J. Kong, H. Dai, *Appl. Phys. Lett.* **2001**, *79*, 3155.
[30] E. Joselevich, C. M. Lieber, *Nano Lett.* **2002**, *2*, 1137.
[31] S. J. Kang, C. Kocabas, T. Ozel, M. Shim, N. Pimparkar, M. A. Alam, S. V. Rotkin, J. A. Rogers, *Nat. Nanotechnol.* **2007**, *2*, 230.
[32] G. Yu, A. Cao, C. M. Lieber, *Nat. Nanotechnol.* **2007**, *2*, 372.
[33] H. Ko, C. Jiang, H. Shulha, V. V. Tsukruk, *Chem. Mater.* **2005**, *17*, 2490.
[34] C. Kocabas, S.-H. Hur, A. Gaur, M. A. Meitl, M. Shim, J. A. Rogers, *Small* **2005**, *1*, 1110.
[35] S. W. Hong, J. Xu, J. Xia, Z. Q. Lin, F. Qiu, Y. L. Yang, *Chem. Mater.* **2005**, *17*, 6223.
[36] J. Xu, J. Xia, S. W. Hong, Z. Q. Lin, F. Qiu, Y. L. Yang, *Phys. Rev. Lett.* **2006**, *96*, 066104.
[37] S. W. Hong, S. Giri, V. S. Y. Lin, Z. Q. Lin, *Chem. Mater.* **2006**, *18*, 5164.
[38] S. W. Hong, J. Xu, Z. Q. Lin, *Nano Lett.* **2006**, *6*, 2949.
[39] S. W. Hong, J. Xia, M. Byun, Q. Zou, Z. Q. Lin, *Macromolecules* **2007**, *40*, 2831.
[40] S. W. Hong, J. Xia, Z. Q. Lin, *Adv. Mater.* **2007**, *19*, 1413.
[41] J. Xu, J. Xia, Z. Q. Lin, *Angew. Chem. Int. Ed.* **2007**, *46*, 1860.
[42] J. Wang, J. Xia, S. W. Hong, F. Qiu, Y. Yang, Z. Q. Lin, *Langmuir* **2007**, *23*, 7411.
[43] M. Byun, S. W. Hong, L. Zhu, Z. Q. Lin, *Langmuir* **2008**, *24*, 3525.
[44] E. Adachi, A. S. Dimitrov, K. Nagayama, *Langmuir* **1995**, *11*, 1057.
[45] R. D. Deegan, O. Bakajin, T. F. Dupont, G. Huber, S. R. Nagel, T. A. Witten, *Nature* **1997**, *389*, 827.
[46] O. Karthaus, L. Grasjo, N. Maruyama, M. Shimomura, *Chaos* **1999**, *9*, 308.
[47] R. D. Deegan, *Phys. Rev. E* **2000**, *61*, 475.
[48] R. D. Deegan, O. Bakajin, T. F. Dupont, G. Huber, S. R. Nagel, T. A. Witten, *Phys. Rev. E* **2000**, *62*, 756.
[49] D.-Q. Yang, J.-F. Rochette, E. Sacher, *J. Phys. Chem. B* **2005**, *109*, 4481.
[50] J. H. Rouse, P. T. Lillehei, *Nano Lett.* **2003**, *3*, 59.
[51] B. Kim, W. M. Sigmund, *Langmuir* **2003**, *19*, 4848.
[52] M. Burghard, V. Krstic, G. S. Duesberg, G. Philipp, J. Juster, S. Roth, *Synth. Met.* **1999**, *103*, 2540.
[53] T. Sainsbury, D. Fitzmaurice, *Chem. Mater.* **2004**, *16*, 2174.
[54] K. Kordas, T. Mustonen, G. Toth, H. Jantunen, M. Lajunen, C. Soldano, S. Talapatra, S. Kar, R. Vajtai, P. M. Ajayan, *Small* **2006**, *2*, 1021.
[55] J. Chen, M. A. Hamon, H. Hu, Y. Chen, A. M. Rao, P. C. Eklund, R. C. Haddon, *Science* **1998**, *282*, 95.

© 2008 WILEY-VCH Verlag GmbH & Co. KGaA, Weinheim